Inorganic Chemistry

Article

pubs.acs.org/IC

Reactivity of an Iron–Oxygen Oxidant Generated upon Oxidative Decarboxylation of Biomimetic Iron(II) α-Hydroxy Acid Complexes

Sayantan Paria, Sayanti Chatterjee, and Tapan Kanti Paine*

Department of Inorganic Chemistry, Indian Association for the Cultivation of Science (IACS), 2A and 2B Raja S. C. Mullick Road, Jadavpur, Kolkata 700032, India

Supporting Information

ABSTRACT: Three biomimetic iron(II) α-hydroxy acid complexes, [(Tp^{Ph2})Fe^{II}(mandelate)(H_2O)] (**1**), [(Tp^{Ph2})-Fe^{II}(benzilate)] (**2**), and [(Tp^{Ph2})Fe^{II}(HMP)] (**3**), together with two iron(II) α-methoxy acid complexes, [(Tp^{Ph2})-Fe^{II}(MPA)] (**4**) and [(Tp^{Ph2})Fe^{II}(MMP)] (**5**) (where HMP = 2-hydroxy-2-methylpropanoate, MPA = 2-methoxy-2-phenylacetate, and MMP = 2-methoxy-2-methylpropanoate), of a facial tridentate ligand Tp^{Ph2} [where Tp^{Ph2} = hydrotris(3,5-diphenylpyrazole-1-yl)borate] were isolated and characterized to study the mechanism of dioxygen activation at the iron(II) centers. Single-crystal X-ray structural analyses of **1**, **2**, and **5** were performed to assess the binding mode of an α-hydroxy/methoxy acid anion to the iron(II) center. While the iron(II) α-methoxy acid complexes are unreactive toward dioxygen, the iron(II) α-hydroxy acid complexes undergo oxidative decarboxylation, implying the importance of the hydroxyl group in the activation of dioxygen. In the reaction with dioxygen, the iron(II) α-hydroxy acid complexes form iron(III) phenolate complexes of a modified ligand (Tp^{Ph2}*), where the ortho position of one of the phenyl rings of Tp^{Ph2} gets hydroxylated. The iron(II) mandelate complex (**1**), upon decarboxylation of mandelate, affords a mixture of benzaldehyde (67%), benzoic acid (20%), and benzyl alcohol (10%). On the other hand, complexes **2** and **3** react with dioxygen to form benzophenone and acetone, respectively. The intramolecular ligand hydroxylation gets inhibited in the presence of external intercepting agents. Reactions of **1** and **2** with dioxygen in the presence of an excess amount of alkenes result in the formation of the corresponding *cis*-diols in good yield. The incorporation of both oxygen atoms of dioxygen into the diol products is confirmed by ^{18}O-labeling studies. On the basis of reactivity and mechanistic studies, the generation of a nucleophilic iron–oxygen intermediate upon decarboxylation of the coordinated α-hydroxy acids is proposed as the active oxidant. The novel iron–oxygen intermediate oxidizes various substrates like sulfide, fluorene, toluene, ethylbenzene, and benzaldehyde. The oxidant oxidizes benzaldehyde to benzoic acid and also participates in the Cannizzaro reaction.

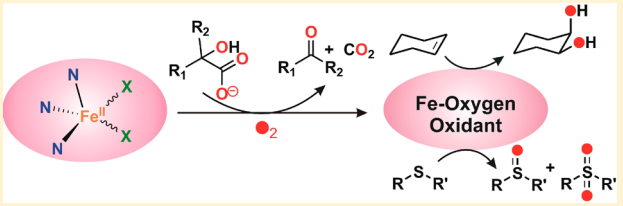

INTRODUCTION

Mononuclear nonheme iron enzymes carry out a variety of metabolically relevant dioxygen-dependent transformation reactions, like aliphatic and aromatic C–C bond cleavage, hydroxylation of alkanes and arenes, halogenation, epoxidation and dihydroxylation of olefins, and oxidation of organosulfur compounds.[1−6] High-valent iron–oxo intermediates, formed upon activation of dioxygen at the iron(II) centers and subsequent cleavage of the O–O bond, have been implicated as the active oxidant to affect these oxidative transformations.[1,7] Iron(IV)–oxo intermediates have been spectroscopically characterized for a number of pterin- and α-ketoglutarate-dependent enzymes.[8−16] Several high-valent iron–oxo species have been isolated and characterized with biomimetic complexes.[17,18] Indirect evidence for an iron(IV)–oxo oxidant was obtained from interception studies with model iron(II) α-keto acid complexes,[19−24] where the α-keto acids provide electrons for dioxygen reduction at the iron center.

The nonheme iron enzymes, Rieske dioxygenases, catalyze the cis-dihydroxylation of arenes in the biodegradation of aromatic compounds.[3,25−30] It is postulated that an iron(V)–oxo–hydroxo oxidant is responsible for the dihydroxylation reaction. An iron(IV)–oxo–hydroxo species has been proposed as the active oxidant in benzoate dioxygenase.[31] However, there is no direct experimental evidence for such an oxidant in the catalytic cycle of Rieske dioxygenases. Inspired by the novel reactions catalyzed by Rieske dioxygenases, a number of nonheme iron complexes have been reported for bioinspired oxidation catalysis.[32−39] The reported complexes have been shown to dihydroxylate or epoxidize olefins with excess hydrogen peroxide. An iron(V)–oxo–hydroxo oxidant has been implicated to carry out the cis-dihydroxylation of aromatic rings in the reaction by a nonheme iron catalyst.[40] Costas et al. have recently shown the existence of an iron(V)–oxo–hydroxo species by variable-temperature mass spectrometry.[41] Que et al. have proposed an iron(IV)–dihydroxy intermediate responsible for olefin cis-dihydroxylation.[34] The presence of "ready oxidant" H_2O_2 and alkene together allows the complex to exhibit catalytic reactivity through a putative

Received: September 26, 2013
Published: March 1, 2014

   dx.doi.org/10.1021/ic402443r | *Inorg. Chem.* 2014, 53, 2810–2821

high-valent iron−oxo oxidant.[42] On the other hand, a supporting reductant is necessary for an oxygen-dependent catalyst that would help to make the "ready oxidant" from aerial oxygen. Examples of high-valent iron−oxo complex formation from molecular oxygen in the presence of a proton and electron donor are, however, rare.[43−47]

While cis-dihydroxylation of olefin is commonly performed by a biomimetic iron complex and H_2O_2, the use of molecular oxygen to perform this reaction remains a challenging task. In this direction, we have recently shown that benzilic acid, an α-hydroxy acid, underwent decarboxylation to form benzophenone in the reaction of an iron(II) benzilate complex with dioxygen.[48] The iron(II) benzilate complex, [(Tp^{Ph2})-Fe^{II}(benzilate)], was capable of cis-dihydroxylation of cyclohexene with the incorporation of both of the oxygen atoms of molecular oxygen into the diol product. In the reaction, the benzilate anion acts as the sacrificial reductant for dioxygen reduction on the iron center.[48] To gain deeper insight into the role of α-hydroxy acids as sacrificial reductants and also to understand the nature of dioxygen-derived oxidant, we have explored the dioxygen reactivity of a series of iron(II) α-hydroxy acid complexes using a monoanionic facial trinitrogen donor ligand, hydrotris(3,5-diphenylpyrazole-1-yl)borate (Tp^{Ph2}). In this Article, we report the dioxygen reactivity of three iron(II) α-hydroxy acid complexes, [(Tp^{Ph2})-Fe^{II}(mandelate)(H$_2$O)] (**1**), [(Tp^{Ph2})Fe^{II}(benzilate)] (**2**), and [(Tp^{Ph2})Fe^{II}(HMP)] (**3**) (HMP = 2-hydroxy-2-methylpropanoate; Scheme 1). We also report the synthesis and reactivity of

Scheme 1. Synthesis of Biomimetic Iron(II) Complexes

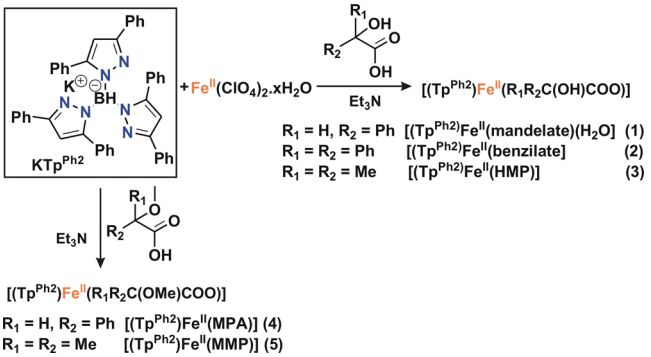

two iron(II) α-methoxy acid complexes, [(Tp^{Ph2})Fe^{II}(MPA)] (**4**) and [(Tp^{Ph2})Fe^{II}(MMP)] (**5**) (where MPA = 2-methoxy-2-phenylacetate and MMP = 2-methoxy-2-methylpropanoate), to compare their reactivity with the iron(II) α-hydroxy acid complexes. The formation of an iron−oxygen intermediate upon dioxygen activation at the metal center of biomimetic iron(II) complexes together with its reactivity toward different substrates is discussed.

EXPERIMENTAL SECTION

All reagents were purchased from commercial sources and used without further purification, unless otherwise noted. Solvents were distilled and dried prior to use. The preparation and handling of air-sensitive materials were carried out under an inert atmosphere by using standard Schlenk techniques or in a glovebox. *Although no problem was encountered during the synthesis of these complexes from Fe(ClO$_4$)$_2$ hydrate, perchlorate salts are potentially explosive and should be handled with care*! KTp^{Ph2} and mandelic-α-*d* acid were prepared according to literature procedures.[49]

Fourier transform infrared spectroscopy on KBr pellets was performed on a Shimadzu FT-IR 8400S instrument. Elemental analyses were performed on a Perkin-Elmer 2400 series II CHN analyzer. Electrospray ionization mass spectrometry (ESI-MS) spectra were recorded with a Waters QTOF Micro YA263 instrument. Solution electronic spectra (single and time-dependent) were measured on an Agilent 8453 diode-array spectrophotometer. All room temperature NMR spectra were recorded on a Bruker Avance 500 MHz spectrometer. Gas chromatography (GC)−MS measurements were carried out on a Perkin-Elmer Clarus 680 gas chromatograph coupled with a Clarus SQ8T mass spectrometer with a maximum temperature of 300 °C using an Elite-5MS (30 m × 0.25 mm × 0.25 μm) column. Labeling experiments were carried out with $^{18}O_2$ gas (99 atom %) from Icon Services Inc..

[Fe^{II}(Tp^{Ph2})(mandelate)(H$_2$O)] (1). To a white slurry of KTp^{Ph2} (0.35 g, 0.5 mmol) and Fe(ClO$_4$)$_2$·6H$_2$O (0.181 g, 0.5 mmol) in methanol (5 mL) was added a methanolic solution (5 mL) of mandelic acid (0.076 g, 0.5 mmol) and triethylamine (70 μL). The resulting milky-white suspension was stirred at room temperature for 2 h. A white solid precipitated and was isolated by filtration and dried. X-ray-quality crystals of **1** were grown from a solvent mixture of dichloromethane and methanol (1:1) at room temperature. Yield: 0.30 g (68%). Elem anal. Calcd for C$_{53}$H$_{43}$BFeN$_6$O$_4$ (894.60 g/mol): C, 71.16; H, 4.84; N, 9.39. Found: C, 70.88; H, 4.91; N, 9.50. IR (KBr): 3400(br), 3034(m), 2623(m), 1717(vs), 16010(br) 1545(m), 1477(m), 1462(m), 1413(m), 1358(m), 1300(m), 1232(m), 1190(m), 1171(m), 1065(s), 1009(m), 939(m), 891(m), 764(s), 731(s), 698(vs), 611(m), 532(m), 517(m) cm^{-1}.

[Fe^{II}(Tp^{Ph2})(mandelate-*d*)] (1-*d*). **1**-*d* was synthesized according to the protocol described for **1** except that mandelic-α-*d* acid was used instead of mandelic acid.

[Fe^{II}(Tp^{Ph2})(benzilate)] (2). Complex **2** was synthesized according to the literature procedure.[48]

[Fe^{II}(Tp^{Ph2})(HMP)] (3). A mixture of 2-hydroxy-2-methylpropanoic acid (0.052 g, 0.5 mmol) and triethylamine (70 μL, 0.5 mmol) in methanol (2 mL) was added to a stirring mixture of the ligand KTp^{Ph2} (0.35 g, 0.5 mmol) and Fe(ClO$_4$)$_2$·6H$_2$O (0.181 g, 0.5 mmol) in methanol (5 mL). The resulting white slurry was allowed to stir at room temperature for 2 h and filtered. The complex was recrystallized from a dichloromethane/methanol solvent mixture. Yield: 0.32 g (77%). Elem anal. Calcd for C$_{49}$H$_{41}$BFeN$_6$O$_3$·CH$_3$OH (860.58 g/mol): C, 69.78; H, 5.27; N, 9.77. Found: C, 69.59; H, 5.30; N, 10.07. IR (KBr): 3583(m), 3462(br), 3063(m), 2623(m), 1545(m), 1477(s), 1464(s), 1431(m), 1414(m), 1358(m), 1335(m), 1236(m), 1172(vs), 1068(m), 1032(m), 1009(m), 968(m), 916(m), 810(m), 764(vs), 698(vs), 671(m), 619(m), 567(m) cm^{-1}.

[Fe^{II}(Tp^{Ph2})(MPA)] (4). Complex **4** was synthesized according to the protocol described for **1** except that α-methoxyphenylacetic acid was used instead of mandelic acid. The crude compound was recrystallized from a solvent mixture of dichloromethane/methanol at room temperature. Yield: 0.32 g (71%). Elem anal. Calcd for C$_{54}$H$_{43}$BFeN$_6$O$_3$ (890.61 g/mol): C, 72.82; H, 4.87; N, 9.44. Found: C, 72.86; H, 4.73; N, 9.27. IR (KBr): 3591(m), 3061(m), 2924(m), 2824(m), 2606(m) 1676(m), 1597(s), 1545(m), 1477(s), 1414(m), 1377(m), 1360(m), 1335(m), 1236(m), 1167(vs), 1119(s), 1068(s), 1007(m), 812(m), 764(vs), 696(vs), 669(m), 631(m), 565(m) cm^{-1}.

[Fe^{II}(Tp^{Ph2})(MMP)] (5). To a stirring solution of KTp^{Ph2} (0.35 g, 0.5 mmol) and Fe(ClO$_4$)$_2$·6H$_2$O (0.181 g, 0.5 mmol) in methanol (5 mL) was added dropwise a mixture of 2-methoxy-2-methylpropanoic acid (0.059 g, 0.5 mmol) and triethylamine (70 μL, 0.5 mmol) in methanol (5 mL). The white slurry was allowed to stir at room temperature for 2 h. The precipitated solid was filtered out, dried under a vacuum, and recrystallized from a dichloromethane/methanol solvent mixture. Yield: 0.28 g (67%). Elem anal. Calcd for C$_{50}$H$_{43}$BFeN$_6$O$_3$ (842.57 g/mol): C, 71.27; H, 5.14; N, 9.97. Found: C, 71.39; H, 4.77; N, 10.14. IR (KBr): 3445(br), 3059(m), 2978(m), 2625(m), 1666(vs), 1545(m), 1479(s), 1464(s), 1414(m), 1377(m), 1030(m), 1009(m), 947(m), 914(m), 874(m), 804(m), 764(vs), 696(vs), 669(m), 567(m) cm^{-1}.

dx.doi.org/10.1021/ic402443r | Inorg. Chem. 2014, 53, 2810−2821

Analyses of Organic Products. The iron(II) complex (0.020 mmol) was dissolved in 10 mL of a dioxygen-saturated organic solvent. The solution was allowed to stir at room temperature. After the reaction, the solution was removed under a vacuum and the residue was treated with 10 mL of a 2 M hydrochloric acid (HCl) solution. The organic products were extracted with diethyl ether (3 × 15 mL), and the organic layer was dried over anhydrous sodium sulfate. After removal of the solvent, the colorless residue was analyzed by GC and ^{1}H NMR spectroscopy. Quantification of benzophenone was done by comparing the peak area of four aromatic ortho protons (δ 7.81 ppm) with respect to the four C−H protons of 1,4-benzoquinone (δ 6.78 ppm) as an internal standard.

Reactions in the Presence of External Substrates. The iron(II) α-hydroxy acid complex (0.02 mmol) was dissolved in 10 mL of benzene under a nitrogen atmosphere, and an external reagent was added. Dioxygen was purged through the solution for 2 min, and the reaction solution was allowed to stir at room temperature for 20−25 min. After oxidation, solvents were removed under reduced pressure and iron complexes were broken by the addition of 10 mL of a 2 M HCl solution. Organic products were extracted by either diethyl ether or chloroform (3 × 15 mL), and the organic layer was dried over anhydrous sodium sulfate. After removal of the solvent, organic products were analyzed by GC−MS and ^{1}H NMR spectroscopy. Quantification of the oxidized organic products were done by the addition of 1,4-benzoquinone (0.02 mmol) as a standard. All of the products were quantified by ^{1}H NMR spectroscopic techniques except benzaldehyde and fluorenone, which were quantified by GC. NMR data of the oxidized products are reported below.

Benzoic acid: ^{1}H NMR (500 MHz, $CDCl_3$) δ 8.18 (d, 2H), 7.63 (t, 1H), 7.48 (t, 2H). Benzaldehyde: ^{1}H NMR (500 MHz, $CDCl_3$) δ 10.02 (s. 1H), 7.53 (t, 2H), 7.63 (t, 1H), 7.88 (d, 2H). Benzyl alcohol: ^{1}H NMR (500 MHz, $CDCl_3$) δ 7.27−7.37 (m, 5H), 4.67 (s, 2H). Benzophenone: ^{1}H NMR (500 MHz, $CDCl_3$) δ 7.80 (d, 4H), 7.59 (t, 2H), 7.50 (t, 4H). 2-Methoxy-2-phenylacetic acid: ^{1}H NMR (500 MHz, $CDCl_3$) δ 7.55 (m, 5H), 4.90 (s, 1H), 3.48 (s, 3H). 2-Methoxy-2-methylpropanoic acid: ^{1}H NMR (500 MHz, $CDCl_3$) δ 3.38 (s, 3H), 1.53 (s, 18H). Thioanisole oxide: ^{1}H NMR (500 MHz, $CDCl_3$) δ 7.66 (m, 2H), 7.52 (m, 3H), 2.73 (s, 3H). Quantification of the products was carried out by comparing the resonance signals for the methyl protons of sulfoxide (at 2.73 ppm) and of sulfone (at 3.06 ppm) with the four C−H protons of 1,4-benzoquinone used as an internal standard.

Methyl phenyl sulfone: ^{1}H NMR (500 MHz, $CDCl_3$) δ 7.96 (d, 2H), 7.60 (m, 3H), 3.06 (s, 3H). Dimethyl sulfoxide: ^{1}H NMR (500 MHz, D_2O) δ 2.74 (s, 6H). Dimethyl sulfone: ^{1}H NMR (500 MHz, D_2O) δ 3.16 (s, 6H). Dibenzothiophene sulfoxide: ^{1}H NMR (500 MHz, $CDCl_3$) δ 8.00 (d, 3H), 7.81 (d, 2H), 7.61 (t, 2H), 7.51 (d, 2H). ^{1}H NMR data were compared with the literature values. *cis*-Cyclohexane-1,2-diol: ^{1}H NMR (500 MHz, $CDCl_3$) δ 3.77−3.82 (m, 2H) 3.58 (br, 2H), 1.73−1.82 (m, 2H), 1.51−1.64 (m, 4H), 1.27−1.35 (m, 2H). 1-Phenylethane-1,2-diol: ^{1}H NMR (500 MHz, $CDCl_3$) δ 7.37 (m, 4H), 7.30 (m, 1H), 4.85 (m, 1H), 3.80 (m, 1H), 3.70 (m, 1H). Octane-1,2-diol: ^{1}H NMR (500 MHz, $CDCl_3$) δ 3.80−3.63 (m, 2H), 3.49 (m, 1H), 1.44−1.40 (m, 2H), 1.30−1.24 (m, 6H), 0.92−0.86 (m, 3H). *cis*-Cyclooctane-1,2-diol: ^{1}H NMR (500 MHz, $CDCl_3$) δ 3.94 (d, 2H), 1.93−1.86 (m, 2H), 1.70−1.63 (m, 4H), 1.55−1.49 (m, 6H). 4-Bromobenzoic acid: ^{1}H NMR (500 MHz, $CDCl_3$) δ 8.00 (d, 2H), 7.61 (d, 2H). 4-Bromobenzyl alcohol: ^{1}H NMR (500 MHz, $CDCl_3$) δ 7.45 (d, 2H), 7.22 (d, 2H), 4.66 (d, 2H).

Quantification of Dimethyl Sulfoxide (DMSO) and Dimethyl Sulfone ($DMSO_2$). The iron(II) complex **1** or **2** (0.02 mmol) was dissolved in benzene (3 mL). Dimethyl sulfide (DMS; 0.02−0.2 mmol) was added to the solution, and dry oxygen was purged through the solution for 2 min. The solution was then allowed to stir for 20−25 min. After the reaction, a mixture of 1,10-phenanthroline (0.06 mmol) and sodium dithionite (0.04 mmol) dissolved in D_2O (0.75 mL) was added, and the solvent mixture was allowed to stir at room temperature for 30 min. The deep-red D_2O layer was allowed to settle, separated, and analyzed by ^{1}H NMR spectroscopy. The organic products were detected by the resonances of the methyl protons at 2.74 and 3.16 ppm for DMSO and $DMSO_2$, respectively. Quantification of the products was done by comparing the six methyl protons of the products with six protons of 2-hydroxy-2-methylpropanoic acid as an internal standard.

X-ray Crystal Structure Determination. X-ray single-crystal data for **1** and **5** were collected at 100 K using Mo Kα (λ = 0.7107 Å) radiation on a SMART-APEX diffractometer equipped with CCD area detector. Crystallographic data of the complexes are presented in Table 1. Data collection, data reduction, structure solution, and refinement were carried out using the software package of *APEX II*.[50] The structure was solved by direct methods and subsequent Fourier analyses and refined by the full-matrix least-squares method based on F^2 with all observed reflections.[51] The non-hydrogen atoms were treated anisotropically. The non-hydrogen atoms were treated anisotropically. The disordered carbon atoms were treated isotropically. The hydrogen atoms were geometrically fixed, except those attached with disordered carbon atoms.

Table 1. Crystallographic Data for 1 and 5

	1	5
empirical formula	$C_{54}H_{43}BCl_2FeN_6O_4$	$C_{51}H_{47}BFeN_6O_4$
fw	977.5	874.61
cryst syst	monoclinic	monoclinic
space group	$P2(1)/n$	$P2/c$
a, Å	10.0685(11)	17.310(4)
b, Å	35.818(4)	9.1759(19)
c, Å	13.2215(14)	29.294(6)
α, deg	90.00	90.00
β, deg	96.132(3)	95.267(7)
γ, deg	90.00	90.00
volume, Å^3	4740.8(9)	4633.2(17)
Z	4	4
$D_{calcd.}$, Mg/m^3	1.370	1.254
μ(Mo Kα), mm^{-1}	0.485	0.376
F(000)	2024	1832
θ range, deg	2.27−18.47	1.18−26.00
reflns collected	25233	40609
reflns unique	4114	8759
R(int)	0.0823	0.0363
data [$I > 2\sigma(I)$]	3278	7706
param refined	619	577
GOF on F^2	1.357	1.212
R1 [$I > 2\sigma(I)$]	0.0626	0.0809
wR2	0.1751	0.2160

RESULTS AND DISCUSSION

The iron(II) complexes were synthesized by mixing the ligand KTp^{Ph2} and iron(II) perchlorate hydrate with basic solutions of α-hydroxy acids or α-methoxycarboxylic acids in methanol (Scheme 1). All of the complexes were purified by recrystallization from a solvent mixture of dichloromethane and methanol. ^{1}H NMR spectra of the iron(II) complexes (**1**−**5**) in benzene-d_6 exhibit paramagnetically shifted proton resonances in the range from +80 to −40 ppm (Figures S1−S4 in the Supporting Information, SI). The binding modes of monoanionic α-hydroxy acids or α-methoxycarboxylic acids to the [$(Tp^{Ph2})Fe^{II}$] unit were established further by single-crystal X-ray structures of **1**, **2**, and **5**.

Single crystals of **1** were grown from a solvent mixture of dichloromethane and methanol. The X-ray crystal structure of the neutral complex **1** displays a five-coordinate iron center ligated by one facial tridentate nitrogen ligand, a monodentate mandelate anion, and a water molecule (Figure 1). The

dx.doi.org/10.1021/ic402443r | Inorg. Chem. 2014, 53, 2810−2821

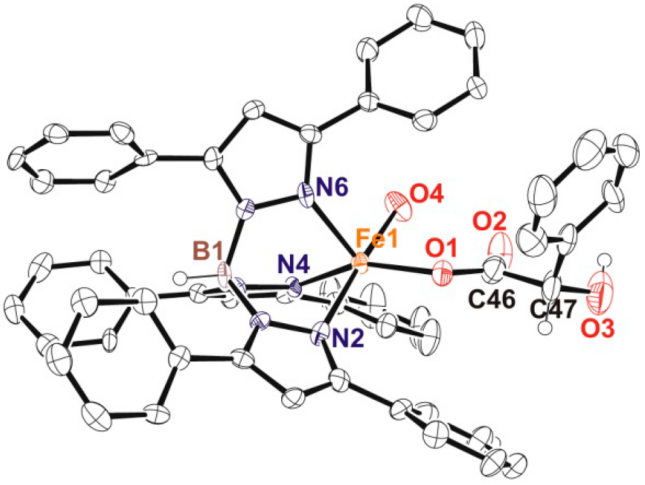

Figure 1. ORTEP diagram of **1** with 50% ellipsoid probability. All hydrogen atoms except those attached to B1, C47, and O3 have been omitted for clarity. Selected bond distances (Å) and angles (deg) for **1**: Fe1–N2 2.168(5), Fe1–N4 2.099(5), Fe1–N6 2.108(5), Fe1–O1 2.002(4), Fe1–O4 2.174(4), C46–O1 1.271(8), C46–O2 1.274(8), C47–O3 1.448(8); N2–Fe1–O4 170.8(2), N6–Fe1–O1 115.2(2), O1–Fe1–O4 89.6(2), N2–Fe1–N4 82.8(2), N6–Fe1–N4 94.7(2), N6–Fe1–N4 91.3(2), N6–Fe1–N2 92.4(2).

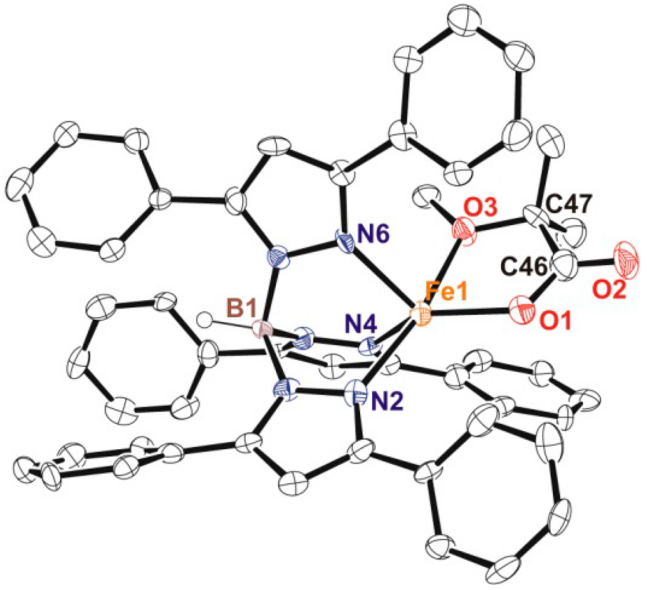

Figure 2. ORTEP plot of **5** with 50% ellipsoid probability. All hydrogen atoms except those attached to B1 have been omitted for clarity. Selected bond distances (Å) and angles (deg) for **5**: Fe1–N2 2.173(3), Fe1–N4 2.102(4), Fe1–N6 2.105(4), Fe1–O1 1.963(3), Fe1–O3 2.227(3), C46–O1 1.285(5), C46–O2 1.240(6), C47–O3 1.445(5); N2–Fe1–O3 167.76(13), N2–Fe1–O1 118.02(13), O1–Fe1–O3 74.11(12), N2–Fe1–N4 97.86(14).

mandelate anion coordinates to the iron center through the carboxylate oxygen (O1) at a distance of 2.002(4) Å. The water oxygen (O4) is coordinated to the iron with a Fe1–O4 distance of 2.174(4) Å. The C47–O3 distance of 1.449 Å is comparable with the C–O bond distance of a secondary alcohol. The binding motif of mandelate, however, differs from the iron(II) α-hydroxy acid complex, [(Tp^{Ph2})Fe^{II}(benzilate)] (**2**), where a bidentate binding of benzilate through the carboxylate oxygen atoms was observed.[48] The presence of phenyl rings on the ligand does not permit coordination of mandelate in a chelating fashion through one carboxylate oxygen and one hydroxyl oxygen. The average Fe–N bond distance of 2.124 Å is comparable to other high-spin (Tp^{Ph2})Fe^{II} complexes.[21,48,52] The iron(II) center in **1** is located in a distorted square-pyramidal coordination geometry (τ = 0.29),[53] where the two pyrazole nitrogen donors (N2 and N4), water oxygen (O4), and carboxylate oxygen (O1) define the basal plane. The pyrazole nitrogen donor (N6) occupies the axial position, with the N6–Fe1–O1, N6–Fe1–O4, N6–Fe1–N4, and N6–Fe1–N2 angles being 115.2(2), 94.7(2), 91.3(2), and 92.4(2)°, respectively. A strong intramolecular hydrogen-bonding interaction is observed between the coordinated water (O4) and noncoordinated carboxylate oxygen (O2) of mandelate with a O···O distance of 2.618 Å.

The iron(II) α-methoxy acid complex **5** was crystallized from a dichloromethane/methanol solvent mixture and crystallizes in a monoclinic space group with one molecule of methanol. Unlike mandelate or benzilate, MMP binds to the iron(II) center in **5** as a bidentate ligand through the carboxylate oxygen (O1) at a distance of 1.963(3) Å and through a methoxy oxygen (O3) at a distance of 2.227(3) Å (Figure 2). The Fe1–O3 distance is almost comparable with the Fe^{II}–O$_{hydroxyl}$ distance in the [(6-Me$_3$-TPA)Fe^{II}(mandelate)]$^+$ complex.[54]

The methyl groups of MMP, being sterically less demanding, likely allow a bidentate coordination mode of MMP to the iron(II) center. A hydrogen-bonding network is present between the noncoordinating carboxylate oxygen (O2) of MMP and a methanol molecule. The three nitrogen atoms of the ligand bind the iron(II) center facially with Fe1–N2, Fe1–N4, and Fe1–N6 distances of 2.173(3), 2.102(4), and 2.105(4) Å, respectively. The average Fe–N distance is comparable with those of **1**, **2**, and other iron(II) complexes of the Tp^{Ph2} ligand.[21,23] The binding mode of the ligand results in a distorted trigonal-bipyramidal (τ = 0.61)[53] coordination geometry at the metal center.

The reactions of iron(II) complexes with dioxygen were carried out in benzene at room temperature. In the reaction with dioxygen, the colorless solution of **1** forms a light-green solution in 20 min. The oxidized solution shows an absorption band at 610 nm in the optical spectrum (Figure 3).

The ESI-MS spectrum of the oxidized solution exhibits ion peaks at m/z 740.2 and 884.2 with the isotope distribution patterns calculated for [(Tp^{Ph2}*)Fe]$^+$ and [{(Tp^{Ph2}*)Fe-(benzoate)}+Na]$^+$, respectively, where Tp^{Ph2}* is a modified form of Tp^{Ph2} in which an *ortho*-carbon of one of the 3-phenyl

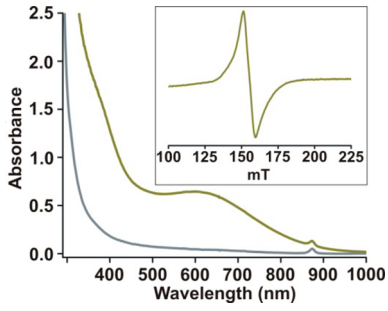

Figure 3. Optical spectra of **1** under a nitrogen environment (gray line) and **1** after reaction with dioxygen (green line) in benzene (concentration = 0.5 mM). Inset: EPR spectrum of the oxidized solution of **1** at 77 K.

dx.doi.org/10.1021/ic402443r | Inorg. Chem. 2014, 53, 2810–2821

rings gets hydroxylated (Figures 4a,b and S5 in the SI). The formation of a green species with the absorbance maximum at

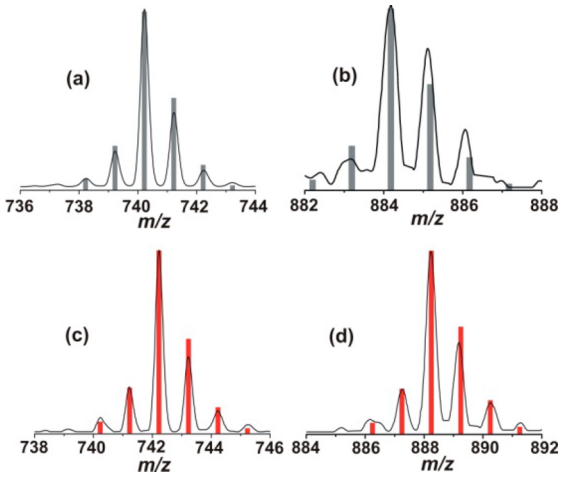

Figure 4. Comparison of ESI-MS of the reaction solution of **1** after reaction with $^{16}O_2$ (a and b) and with $^{18}O_2$ (c and d). Red bars indicate the corresponding computer-simulated spectra.

650 nm has been reported for a number of related $Fe^{II}Tp^{Ph2}$ complexes in the reaction with dioxygen.[21,23,55] The X-band electron paramagnetic resonance (EPR) spectrum of the greenish solution at 77 K exhibits a rhombic signal at $g = 4.3$ (Figure 3, inset), indicating that **1**, after reaction with oxygen, converts to a high-spin iron(III) complex of the Tp^{Ph2}* ligand. On the basis of the reported molar extinction coefficient of $[(Tp^{Ph2}*)Fe(benzoate)]$,[21] about 88% of ligand hydroxylation is estimated in the reaction. Analyses of organic products derived from mandelate reveal the formation of 20% benzoic acid, 67% benzaldehyde, and 10% benzyl alcohol (Scheme 2 and Figure S6 in the SI). The latter two products were analyzed and quantified by GC and GC−MS.

Scheme 2. Organic Products Derived from the Iron(II) α-Hydroxy Acid Complexes

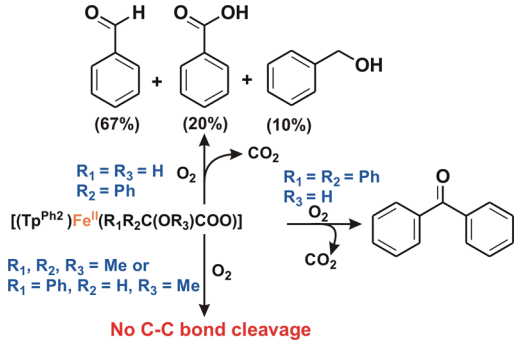

On the other hand, complex **2**, where no α-hydrogen atom is present in benzilate, reacts with dioxygen within 15 min to exhibit 90% ligand hydroxylation.[48] In the oxidation reaction, benzilate is quantitatively decarboxylated to benzophenone. Similarly, complex **3** takes 4 h to decarboxylate HMP to acetone quantitatively, where nearly 80% ligand hydroxylation is observed (Figures S7 and S8 in the SI).

ESI-MS of the solutions after reaction of **1** and **2** with $^{18}O_2$ in benzene displays an ion peak at m/z 742.2 (Figure 4c), indicating that one labeled oxygen from $^{18}O_2$ is incorporated into the hydroxylated ligand. Additionally, the ion peak at m/z 884.2 observed in **1** is shifted four mass units higher to m/z 888.2 (Figures 4d and S9 in the SI), strongly supporting the incorporation of another labeled oxygen atom into benzoic acid. The GC−MS spectrum of benzyl alcohol derived from **1** shows an ion peak at m/z 108 (Figure 5a). When the reaction is

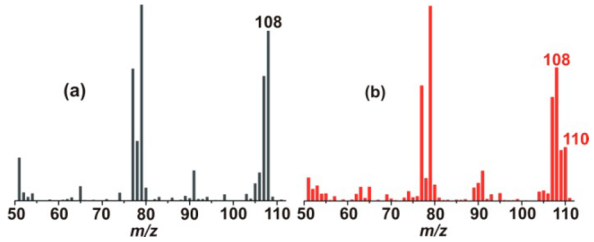

Figure 5. GC−MS spectra of benzyl alcohol derived from **1** after reaction with (a) $^{16}O_2$ and (b) $^{18}O_2$.

carried out in the presence of $^{18}O_2$, the peak is shifted to m/z 110 with about 30% incorporation of labeled oxygen into benzyl alcohol (Figure 5b). However, the carbonyl products derived from α-hydroxy acids do not contain any labeled oxygen, as confirmed by GC−MS analysis.

It is clear from the dioxygen reactivity of **1**−**3** that all of the α-hydroxy acids undergo oxidative decarboxylation to form the corresponding carbonyl compounds (Scheme 2). However, the distribution of organic products derived from complex **1** is surprisingly different. Compared to the product derived from **2** and **3**, benzaldehyde is expected to be the only product from **1**. Although benzaldehyde is found to be the major product, benzoic acid and benzyl alcohol are the other two products derived from mandelic acid. Despite the difference in the reactivity of the iron(II) α-hydroxy acid complexes, the presence of an O−H group is common in all of these complexes. To check the role of the O−H group in the decarboxylation reactions, the dioxygen reactivities of two iron(II) α-methoxy acid complexes were tested for comparison. MPA has no O−H bond but has one α-C−H bond, whereas MMP has neither an α-C−H bond nor an O−H bond. The iron(II) α-methoxy acid complexes, **4** and **5**, do not react with oxygen, implying the role of the O−H group for oxidative decarboxylation of α-hydroxy acids (Scheme 2 and Figures S10−S12 in the SI).

The formation of benzoic acid and concomitant ring hydroxylation of the Tp^{Ph2} ligand have been reported for the iron(II) benzoylformate complex, $[(Tp^{Ph2})Fe^{II}(benzoylformate)]$.[21] A high-spin Fe^{IV}=O oxidant, responsible for aromatic ring hydroxylation, was intercepted by external reagents. While no iron−oxygen intermediate was directly observed with the present systems for spectroscopic characterization, studies have been performed with **1** and **2** in the presence of external substrates to intercept the active oxidant (Chart 1). In the interception experiments, the charge-transfer (CT) band of $[(Tp^{Ph2}*)Fe^{III}]^+$ was used as a probe to monitor the interception of the active oxidant.

Different sulfides like thioanisole, DMS, and dibenzothiophene (DBT) were used for interception studies (Chart 1). In the presence of sulfides, oxidative C−C bond cleavage of mandelate or benzilate takes place quantitatively. However, the percentage of ligand hydroxylation varies with varying amounts of thioanisole (Figures 6 and S13 in the SI). The reaction of **1** with dioxygen in the presence of 1 equiv of thioanisole exhibits

dx.doi.org/10.1021/ic402443r | Inorg. Chem. 2014, 53, 2810−2821

Chart 1. Reagents Used To Intercept the Iron−Oxygen Oxidant

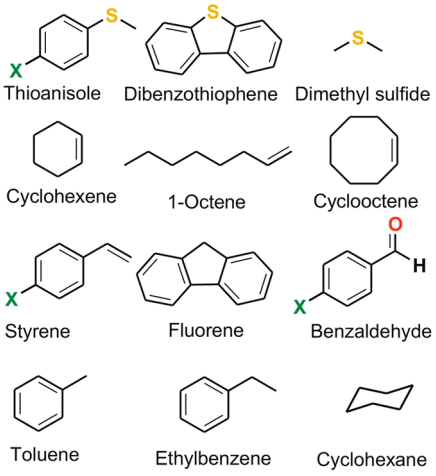

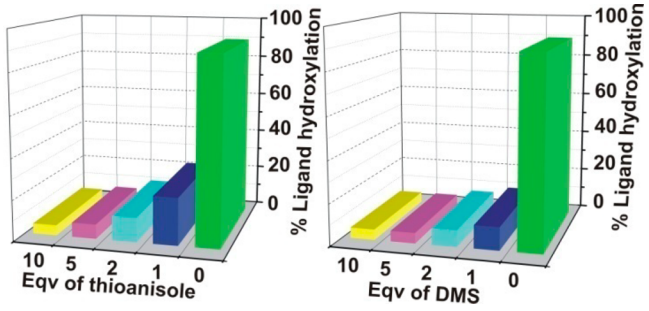

Figure 6. Extent of ligand hydroxylation in the reaction of **1** with dioxygen in the presence of 1−10 equiv of thioanisole and DMS.

about 20% ligand hydroxylation. When 10 equiv of thioanisole is used, only 5% ligand hydroxylation is observed. In the latter, 80% thioanisole oxide and 10% methyl phenyl sulfone are formed (Scheme 3 and Figure S14 in the SI). Importantly, with

Scheme 3. Interception of the Iron−Oxygen Oxidant Using Different Sulfides[a]

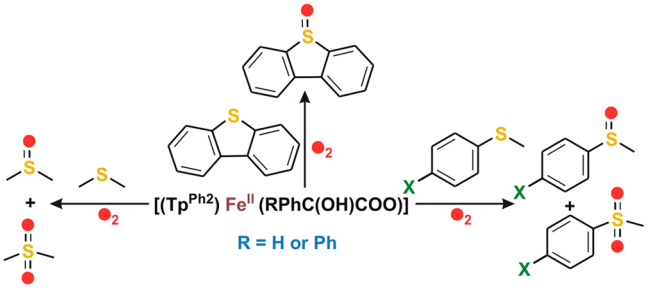

[a]The products derived from mandelate and benzilate are not shown here.

a decreasing amount of thioanisole, the amount of sulfone formation increases, while the yield of sulfoxide decreases (Table S1 in the SI). With 1 equiv of thioanisole, 34% sulfone is observed as the only product with no sulfoxide. Thus, the distribution of thioanisole-derived products strongly depends on the initial concentration of thioanisole. The ESI-MS spectrum of the oxidized species after the reaction of **1** with dioxygen and excess thioanisole displays an ion peak at m/z 725.2, with the isotope distribution pattern calculated for $[(Tp^{Ph2})Fe]^+$ supporting the theory that the ligand backbone remains unaffected (Figure S15 in the SI). An excess amount of sulfides intercepts the active oxidants and thereby inhibits the ring hydroxylation pathway. In the case of **2**, as expected, the distribution of thioanisole-derived products mirrors the result obtained with complex **1**.

To assess the source of oxygen atoms in thioanisole-derived products, ^{18}O-labeling experiments were carried out with complex **1** in the presence of 2 equiv of thioanisole. GC−MS spectra of the organic products display ion peaks at m/z 140 and 156 corresponding to $[C_6H_5SO^{16}CH_3]^{\cdot+}$ (Figure 7a) and $[C_6H_5SO_2{}^{16}CH_3]^{\cdot+}$ (Figure 7b) that shift to m/z 142 (Figure 7c) and m/z 160 (Figure 7d), respectively, in the presence of $^{18}O_2$. Therefore, the theory that the oxygen atoms in thioanisole-derived products originate from molecular oxygen.

Similar to thioanisole, DMS affects ring hydroxylation in both **1** and **2**. With 10 equiv of DMS, ligan hydroxylation takes place only to an extent of 5% with both complexes. When the amount of DMS is reduced to 1 equiv, around 15% of ligand hydroxylation is estimated for both complexes (Table S1 in the SI and Figure 6). The products derived from DMS after oxidation were analyzed by ^{1}H NMR spectroscopy in D_2O (see the Experimental Section and Figure S16 in the SI). The percentage of $DMSO_2$ decreases with an increase in the DMS concentration. DBT was also found to intercept the oxidant from both **1** and **2** (Figures 8 and S13 in the SI). As observed with thioanisole and DMS, DBT inhibits ligand hydroxylation almost quantitatively. In the reactions with DBT, however, dibenzothiophene sulfoxide is found to be the only product (Table S1 and Figures S17 and S18 in the SI). There may be two factors that control the product distribution: the concentration and the steric effect of sulfide. In a crossover experiment, it is observed that **1** (and **2**) prefers to oxidize thioanisole when equimolar amounts of thioanisole and DBT are present in the reaction mixture (Figure S19 in the SI). When a mixture of thioanisole and thioanisole oxide is present, thioanisole oxide preferentially gets oxidized to sulfone.

The oxidation of sulfide to sulfoxide is a well-known reaction that takes place in the presence of a high-valent iron−oxo intermediate. A variety of synthetic iron(IV) oxo complexes have been shown to oxidize thioanisole to thioanisole oxide.[56,57] A high-spin iron(III)−hydroperoxo intermediate has also been proposed to oxidize sulfide to sulfoxide.[58] The two-electron oxidative decarboxylation of α-hydroxy acids in **1** and **2** rules out the involvement of an iron(III)−hydroperoxo or superoxo species. The observed oxidation of thioanisole to a mixture of thioanisole oxide and methyl phenyl sulfone suggests that the nature of the iron−oxygen species from **1** and **2** must be different from those reported. A Hammett analysis would provide useful information regarding the nature of the active oxidant. Because the intermediate is not observed, no absolute reaction rate can be obtained. However, relative rates can be obtained from product analysis of the competition oxidation of pairs of sulfides. For Hammett analysis with complex **2**, competitive reactions were carried out with 1:1 mixtures of thioanisole and different para-substituted thioanisoles (*p*-$XPhSCH_3$, where X = NO_2, Cl, H, Me, OMe). A ρ value of +0.88 was obtained from the Hammett plot of the relative rates (k_{rel}) versus σ_p^+ (Figure 8). The data clearly indicate that the oxidant responsible for oxygen-atom transfer to thioanisole has nucleophilic character.

dx.doi.org/10.1021/ic402443r | Inorg. Chem. 2014, 53, 2810−2821

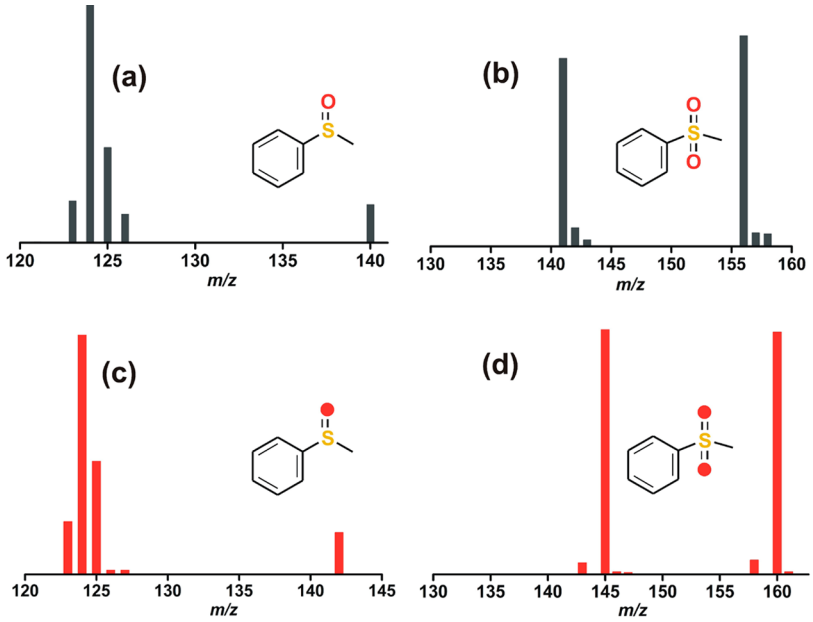

Figure 7. Thioanisole-derived products after the reaction of complex **1** with $^{16}O_2$ (a and b) and $^{18}O_2$ (c and d).

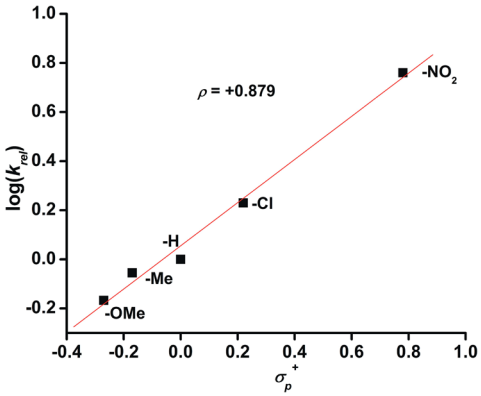

Figure 8. Hammett plot of log k_{rel} versus σ_p^+ for *p*-XPhSCH$_3$. The k_{rel} value was calculated by dividing the concentration of the product from *p*-XPhSCH$_3$ by the concentration of the product from PhSCH$_3$.

For further insight into the nature of active oxidant generated from **1** and **2**, interception experiments were carried out in the presence of 100 equiv of cyclohexene. Ligand hydroxylation occurs only up to 5−6% for **1** and 10% for **2** (Figures 9 and S20 in the SI).[48] ^{1}H NMR spectral analyses of organic products reveal the formation of 70% *cis*-cyclohexane-1,2-diol as the only product with complex **1** (Scheme 4 and Figure S21 in the SI).

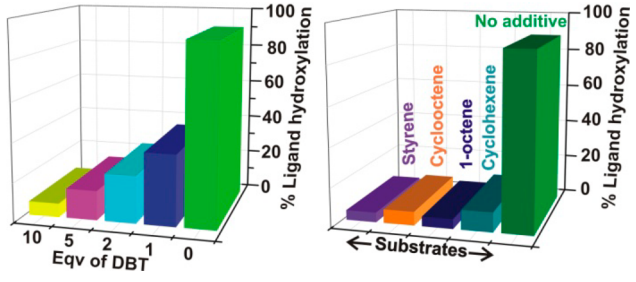

Figure 9. Extent of ligand hydroxylation in the reaction of **1** with dioxygen in the presence of 1−10 equiv of DBT (left) and 100 equiv of different alkenes (right).

Scheme 4. Oxidation Products of Different Alkenes in the Reactions of 1 and 2 with Dioxygen

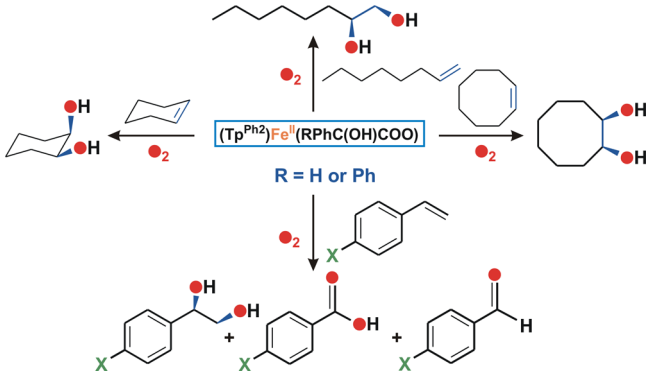

The yield of *cis*-cyclohexane-1,2-diol is found to be 60% in the case of **2**.[48] The ESI-MS spectra of the oxidized solutions of **1** or **2** in the presence of cyclohexene show a predominant peak at *m*/*z* 841.3, which corresponds to a composition of $\{[(Tp^{Ph2})Fe(C_6H_{11}O_2)]+H\}^+$, indicating the binding of *cis*-diol to the metal center (Figure S22 in the SI). Importantly, with complex **1**, the yield of benzoic acid is reduced to 12% and that of benzaldehyde is increased to 75% in the presence of cyclohexene. Moreover, no benzyl alcohol is observed in the reaction.

Labeling experiments using $^{18}O_2$ strongly support the incorporation of both atoms of molecular oxygen into the *cis*-diol product. The GC−MS spectrum of the *cis*-diol exhibits a predominant peak at *m*/*z* 116 attributable to $[C_6H_{12}O_2]^+$. The *m*/*z* value is shifted to four units higher at *m*/*z* 120 in the presence of $^{18}O_2$ (Figure 10). The results strongly support the theory that the O_2-derived oxidant from the iron(II) α-hydroxy acid complexes is capable of transferring both oxygen atoms to cyclohexene. A mixed labeling experiment with $^{16}O_2$ in the presence of H_2O^{18} confirms no incorporation of labeled oxygen into the *cis*-diol product. The amount of diol product reduces in the presence of proton donors like pyridinium/lutidinium perchlorate or a proton acceptor like pyridine.

dx.doi.org/10.1021/ic402443r | Inorg. Chem. 2014, 53, 2810−2821

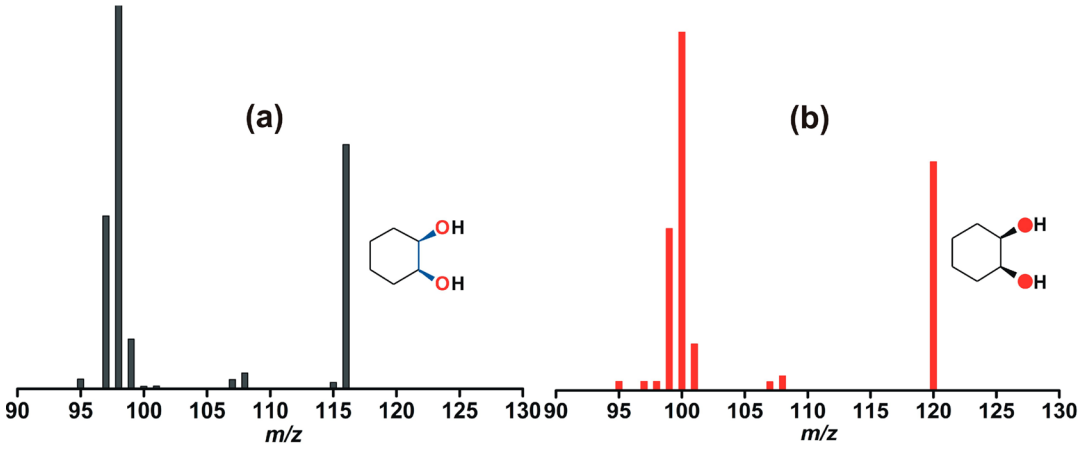

Figure 10. GC−MS spectra of *cis*-cyclohexane-1,2-diol formed in the reaction of **1** with (a) $^{16}O_2$ and (b) $^{18}O_2$ in the presence of 100 equiv of cyclohexene.

Other alkenes like 1-octene, cyclooctene, and styrene are also capable of intercepting the oxidant from **1** and **2** almost quantitatively (Figure 9). When 1-octene is used as a substrate, the formation of octane-1,2-diol is observed in 85% yield with both complexes (Scheme 4 and Figures S23 and S24 in the SI). The ESI-MS spectrum of the oxidized solution shows a peak at m/z 871.3 corresponding to a composition of $\{[(Tp^{Ph2})Fe(C_8H_{17}O_2)]+H\}^+$ (Figure S25 in the SI). In the presence of cyclooctene, 80% *cis*-cyclooctane-1,2-diol is observed (Figures S26 and S27 in the SI).

Unlike other alkenes, styrene affords 1-phenylethane-1,2-diol, benzaldehyde, and benzoic acid as products in the reaction of **2** (Scheme 4 and Figures 11 and S28 in the SI). Interestingly, the

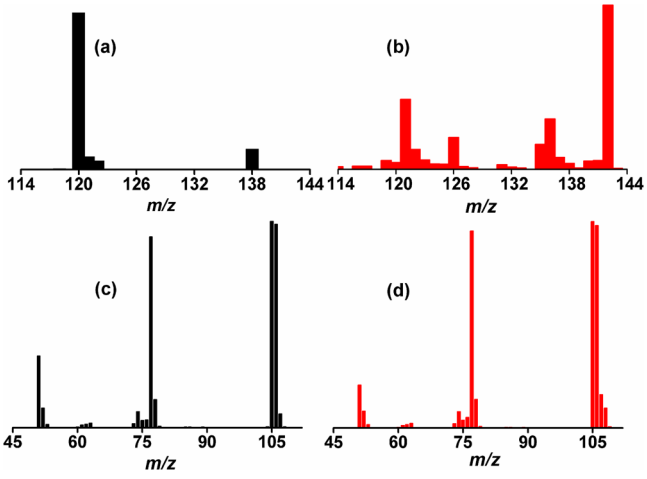

Figure 11. GC−MS spectra of the products derived from styrene in the reaction of **1** with $^{16}O_2$ (a and c) and $^{18}O_2$ (b and d).

yields of benzaldehyde and benzoic acid increase, whereas the yield of diol decreases with time. At the end of the reaction after 20 min, nearly 20% diol, 50% benzaldehyde, and 30% benzoic acid are formed. The ESI-MS spectrum of the oxidized solution shows an ion peak at m/z 863.3 attributable to $\{[(Tp^{Ph2})Fe(C_8H_9O_2)]+H\}^+$ (Figure S29 in the SI). The ion peak is shifted four mass units higher at m/z 867.3 (Figure S30 in the SI) when the reaction is carried out with $^{18}O_2$.

The GC−MS spectrum of the diol derived from the reaction of **1** with $^{16}O_2$ in the presence of styrene shows an ion peak at m/z 138 (Figure 11a) corresponding to $[C_8H_{10}O_2]^+$. The m/z value is shifted four mass units higher to m/z 142 (Figure 11b) in the presence of $^{18}O_2$. The GC−MS spectrum of benzaldehyde in the ^{18}O-labeling experiment shows peaks at m/z 106 and 108 (Figure 11d). The peaks indicate that a part of benzaldehyde is derived from mandelate and another part is derived from 1-phenylethane-1,2-diol. Benzoic acid from mandelate displays an ion peak at m/z 124, while benzoic acid derived from 1-phenylethane-1,2-diol shows an ion peak at m/z 126 in the GC−MS spectrum (Figure S31 in the SI). These results support the iron-mediated oxidative C−C bond cleavage of 1-phenylethane-1,2-diol. The formation of benzoic acid in an independent reaction of 1-phenylethane-1,2-diol with $[(Tp^{Ph2})Fe(formate)]$ further confirmed the C−C bond cleavage of the diol.

The use of molecular oxygen in generating an oxidizing species capable of performing cis-dihydroxylation of olefin is quite intriguing. Hammett analysis was performed by product analysis of the competition oxidation of pairs of styrenes to evaluate the nature of the oxidant. For Hammett analysis, competitive reactions were carried out with 1:1 mixtures of styrene and different para-substituted styrenes (p-XPhCH=CH_2, where X = CN, Cl, H, Me, OMe). A ρ value of +0.95 was obtained from the Hammett plot of the relative rates (k_{rel}) versus σ_p^+ for p-XPhCH=CH_2 (Figure 12). The result strongly indicates that the intermediate responsible for cis-dihydroxylation of styrene has nucleophilic character.

The oxidation of alkene to *cis*-diol takes place only in the presence of an oxidant with two oxygen atoms disposed in a cis position as in osmium tetroxide, potassium permanganate, etc.[59] Hammett analyses on sulfides and alkenes suggest the nucleophilic nature of the oxidant derived from the α-hydroxy acid complexes (**1** and **2**). Quantitative oxidations of α-hydroxy acids to the corresponding carbonyl compounds suggest two-electron reduction of dioxygen, and the oxidant is expected to be a side-on iron(II) hydroperoxo species. The iron(II) hydroperoxo species may also undergo O−O bond heterolysis to form an iron(IV)−oxo−hydroxo species. High-valent iron−oxo intermediates have been reported to show electrophilic character and can exchange their oxygen atoms with water. On the contrary, the *cis*-diol products obtained in the reactions of alkenes with **1** (or **2**) derive both oxygen atoms from molecular oxygen, and the oxidant does not exchange its oxygen atoms with water. An iron(IV)−oxo−hydroxo oxidant is likely to exchange its oxygen atoms with water. However, a high-spin

dx.doi.org/10.1021/ic402443r | Inorg. Chem. 2014, 53, 2810−2821

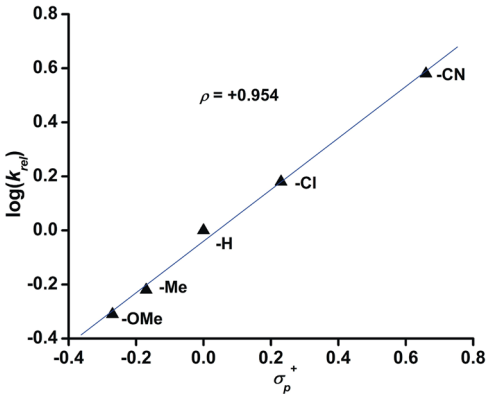

Figure 12. Hammett plot of log k_{rel} versus σ_p^+ for *p*-XPhCH=CH_2. The k_{rel} value was calculated by dividing the concentration of the product from para-substituted styrene by the concentration of the product from styrene.

iron(IV)−oxo−hydroxo species has not been isolated so far, so its chemical behavior is not known. Furthermore, Que et al. have reported a nucleophilic oxidant from [(6-Me_3-TPA)Fe-$(OTf)_2$] responsible for catalytic cis-hydroxylation of alkenes in the presence of H_2O_2, where both oxygen atoms of the diols are derived from H_2O_2.[60] Therefore, the active oxidant generated in the oxidative decarboxylation of the iron(II) mandelate/benzilate complex could be either an iron(II)−hydroperoxo or an iron(IV)−oxo−hydroxo species.

Complex **1** reacts with 100 equiv of fluorene to exhibit 35% ligand hydroxylation and quantitative decarboxylation of mandelate (Figure S32 in the SI). In the reaction, 60% fluorenone is formed (Figure S33 in the SI). The yield of fluorenone with **2** is slightly lower than that observed with **1** under similar experimental conditions.[48] Toluene and ethylbenzene are found to intercept the active oxidant from **2** to exhibit 42% and 47% ligand hydroxylation, respectively. While toluene yields benzyl alcohol (16%) and benzaldehyde (40%) (Scheme 5 and Figure S34 in the SI), ethylbenzene affords 13% 1-phenylethanol and 38% acetophenone (Figures S35 and S36 in the SI). However, substrates containing strong C−H bonds like cyclohexane (100 equiv) are found to have no effect on ligand hydroxylation.

As mentioned before, complex **1** afforded benzaldehyde as the major product. Analyses of organic products reveal decarboxylation of mandelic acid to benzaldehyde (82%), benzoic acid (9%), and benzyl alcohol (3%) in 5 min. However, the product distribution changes with time with the formation of 78% benzaldehyde, 15% benzoic acid, and 4% benzyl alcohol in 10 min. After 15 min, the reaction affords 67% benzaldehyde, 20% benzoic acid, and 10% benzyl alcohol. The time-dependent product distribution profile supports the formation of benzoic acid and benzyl alcohol from benzaldehyde. In search of a possible mechanism for the formation of benzyl alcohol and benzoic acid, products were analyzed after oxygenation of [$(Tp^{Ph2})Fe^{II}$(mandelate-*d*)] (**1**-*d*). In the ^1H NMR spectrum, the intensity of the peak due to methylene protons of benzyl alcohol at 4.7 ppm is decreased considerably, whereas the resonance for the C−H proton of benzaldehyde has completely vanished at 10.02 ppm (Figure S37 in the SI). The ion peak at *m*/*z* 110 with the mass fragmentation patterns in the GC−MS spectrum confirms the formation of $C_6H_5CD_2OH$ (Figure 13). The ion peak at *m*/*z* 107 is

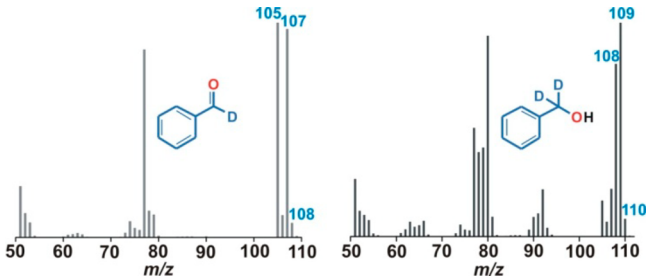

Figure 13. GC−MS spectra of benzyl alcohol and benzaldehyde derived from the reaction of **1**-*d* with oxygen.

attributable to PhCDO (Figure 13). The source of benzaldehyde is mandelate, and the alcohol is formed via hydride migration from benzaldehyde through the Cannizzaro reaction. Accordingly, we propose that benzaldehyde formed from **1** undergoes a Cannizzaro-type reaction, resulting in the formation of equivalent amounts of benzyl alcohol and benzoic acid (Scheme 5).

The yield of benzoic acid is, however, found to be higher than that of benzyl alcohol. It is likely that the nucleophilic iron−oxygen oxidant oxidizes benzaldehyde to benzoic acid. When the reaction of **2** is carried out with 20 equiv of benzaldehyde, ligand hydroxylation takes place to an extent of 35% and, in the reaction, nearly 40% benzyl alcohol and 75−80% benzoic acid are formed (Scheme 5 and Figure S38 in the SI). The GC−MS spectrum of benzyl alcohol (Figure 14) supports the partial incorporation of ^{18}O into benzyl alcohol. Moreover, the peak at *m*/*z* 124 (Figure 14) indicates the incorporation of labeled oxygen into benzoic acid. In the presence of 20 equiv of 4-bromobenzaldehyde, the reaction of **2** with dioxygen affords 85% 4-bromobenzoic acid and 40% 4-

Scheme 5. Oxidation Products of Different Substrates from the Reaction of 2 with Dioxygen

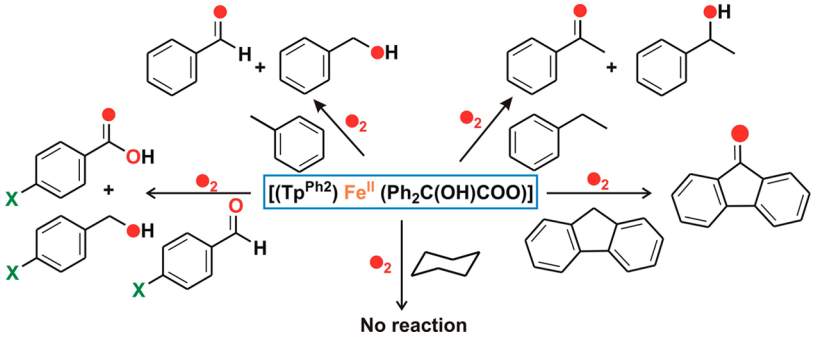

dx.doi.org/10.1021/ic402443r | Inorg. Chem. 2014, 53, 2810−2821

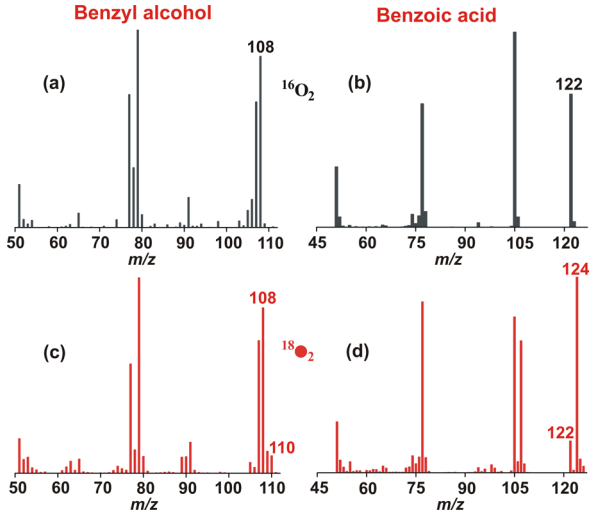

Figure 14. GC–MS spectra of Cannizzaro products from benzaldehyde in the reaction of **2** with $^{16}O_2$ and $^{18}O_2$.

bromobenzyl alcohol with 25% ligand hydroxylation (Figures S39 and S40 in the SI).

All of these results support the existence of two pathways for benzoic acid formation from **1**. The metal-based oxidant oxidizes benzaldehyde (10%) to benzoic acid, and the resulting iron(II) hydroxo species participates in the Cannizzaro reaction to convert benzaldehyde (20%) into benzyl alcohol (10%) and benzoic acid (10%) (Scheme 6). An estimated 30% of the total benzaldehyde takes part in these two pathways. The metal-bound hydroxide attacks the electrophilic center of benzaldehyde, forming a *gem*-diol adduct that may exist in equilibrium with the aldehyde. The existence of such an equilibrium is supported by the fact that a small percentage of the incorporation of one labeled oxygen atom into benzyl alcohol takes place in the reaction of **1** with $^{18}O_2$.

On the basis of the reactivity studies described above, it is proposed that an iron(III) superoxide species, formed initially upon activation of O_2 at the iron(II) center, abstracts the hydrogen atom from the O–H group of α-hydroxy acid (Scheme 7). The iron(III) hydroperoxo species with a coordinated radical then rearranges to an iron(II) hydroperoxo via decarboxylation of the α-hydroxy acid to the corresponding carbonyl compound. The iron(II) hydroperoxo species may also undergo O–O bond heterolysis to form an iron(IV)–oxo–hydroxo intermediate. Either of these two oxidants carries out the oxidation of various substrates. In the absence of any external substrate, the oxidant species hydroxylates one of the 3-phenyl rings of the Tp^{Ph2} ligand. The resulting iron(II) phenolate complex readily reacts with the residual O_2 and gets oxidized to an iron(III) phenolate species exhibiting a broad CT band at 600 nm for **2** and 610 nm for **1**. Oxidation of complex **1** yields a mixture of benzoic acid (20%), benzaldehyde, and benzyl alcohol, where benzoic acid may easily replace the hydroxide ion to form an $Fe^{III}(Tp^{Ph2*})$-(benzoate) complex. A mixture of iron(III) benzoate and iron(III) hydroxide exhibits a CT band in the range of 600–650 nm depending on the percentage of two iron(III) phenolate products. The oxidized solution after the reaction of **1** with dioxygen and 20 equiv of benzaldehyde exhibits a chromophore at 640 nm (Figure S41 in the SI). The band is shifted considerably toward 650 nm because a higher concentration of benzoate results in a higher amount of iron(III) phenolate benzoate species responsible for the green color. While the oxidant from the iron(II) benzoylformate complex of the Tp^{Ph2} ligand shows shape-selective oxidation of substrates,[55] the oxidant generated from the iron(II) α-hydroxy acid complexes exhibits versatile reactivity toward organic substrates.

CONCLUSION

We have reported the synthesis, characterization, and dioxygen reactivity of a series of biomimetic iron(II) α-hydroxy acid complexes supported by a facial trinitrogen ligand. The iron(II) α-hydroxy acid complexes react with dioxygen to undergo oxidative decarboxylation of α-hydroxy acids, resulting in the formation of the corresponding carbonyl compounds. The iron(II) α-methoxy acid complexes are found to be unreactive toward dioxygen and indicate the importance of the O–H group to initiate the C–C bond cleavage reaction by an iron(III)–superoxide intermediate. The oxidant generated in oxidative decarboxylation of α-hydroxy acids could be

Scheme 6. Proposed Mechanism for the Oxidation of Benzaldehyde by the Oxidant Generated from Iron(II) α-Hydroxy Acid Complexes in the Reaction with Dioxygen

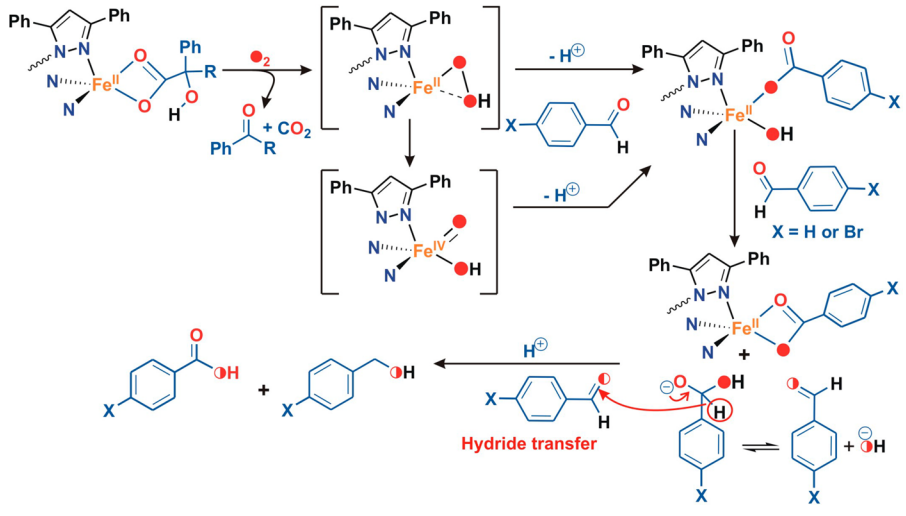

dx.doi.org/10.1021/ic402443r | *Inorg. Chem.* 2014, 53, 2810–2821

Scheme 7. Proposed Pathway for the Formation of an Iron−Oxygen Oxidant upon Oxidative Decarboxylation of α-Hydroxy Acids

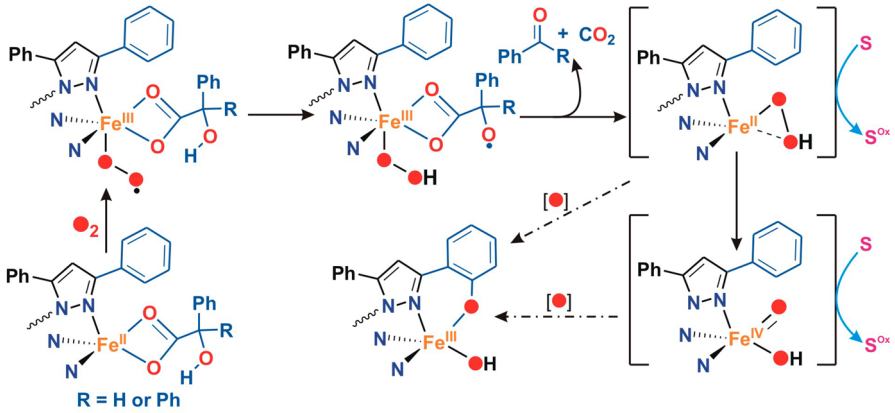

intercepted by different substrates. The nucleophilic iron−oxygen oxidant is capable of converting alkenes to *cis*-diols with both oxygen atoms derived from dioxygen. The novel oxidant exhibits versatile reactivity like oxygen-atom transfer to sulfides, aliphatic C−H bond activation, and olefin cis-dihydroxylation. In the absence of any substrate, the oxidant intramolecularly hydroxylates one of the phenyl rings on the ligand. The active oxidant could either be an iron(II)−hydroperoxo or an iron(IV)−oxo−hydroxo species. However, further mechanistic investigation is required to understand the exact nature of the dioxygen-derived oxidant. The iron(II) α-hydroxy acid complexes represent the functional models of Rieske dioxygenases where the iron-coordinated α-hydroxy acid anions provide the necessary electrons and protons for dioxygen reduction to form the active oxidant. The results described herewith would provide useful insight into the development of a bioinspired oxidation catalyst for olefin cis-hydroxylation using dioxygen as the oxidant in the presence of sacrificial reductants.

■ ASSOCIATED CONTENT

Ⓢ Supporting Information

Crystallographic data in CIF format, product distribution table, electronic spectra, and ESI-MS, GC−MS, and NMR spectra. This material is available free of charge via the Internet at http://pubs.acs.org.

■ AUTHOR INFORMATION

Corresponding Author

*E-mail: ictkp@iacs.res.in. Tel: +91-33-2473-4971. Fax: +91-33-2473-2805.

Author Contributions

S.P. and S.C. contributed equally to this work.

Notes

The authors declare no competing financial interest.

■ ACKNOWLEDGMENTS

The authors thank the Department of Science and Technology (DST), Government of India, for financial support (Project SR/SI/IC-51/2010). S.P. and S.C. thank the Council of Scientific and Industrial, India, for fellowships. X-ray diffraction data were collected at the DST-funded National Single Crystal Diffractometer Facility at the Department of Inorganic Chemistry, IACS.

■ REFERENCES

(1) Costas, M.; Mehn, M. P.; Jensen, M. P.; Que, L., Jr. *Chem. Rev.* **2004**, *104*, 939.
(2) Bruijnincx, P. C. A.; van Koten, G.; Gebbink, R. J. M. K. *Chem. Soc. Rev.* **2008**, *37*, 2716.
(3) Kovaleva, E. G.; Lipscomb, J. D. *Nat. Chem. Biol.* **2008**, *4*, 186.
(4) Hausinger, R. P. *Crit. Rev. Biochem. Mol. Biol.* **2004**, *39*, 21.
(5) Solomon, E. I.; Decker, A.; Lehnert, N. *Proc. Natl. Acad. Sci. U.S.A.* **2003**, *100*, 3589.
(6) Solomon, E. I.; Brunold, T. C.; Davis, M. I.; Kemsley, J. N.; Lee, S.-K.; Lehnert, N.; Neese, F.; Skulan, A. J.; Yang, Y.-S.; Zhou, J. *Chem. Rev.* **2000**, *100*, 235.
(7) Krebs, C.; Fujimori, D. G.; Walsh, C. T.; Bollinger, J. M., Jr. *Acc. Chem. Res.* **2007**, *40*, 484.
(8) Price, J. C.; Barr, E. W.; Tirupati, B.; Bollinger, J. M., Jr.; Krebs, C. *Biochemistry* **2003**, *42*, 7497.
(9) Proshlyakov, D. A.; Henshaw, T. F.; Monterosso, G. R.; Ryle, M. J.; Hausinger, R. P. *J. Am. Chem. Soc.* **2004**, *126*, 1022.
(10) Riggs-Gelasco, P. J.; Price, J. C.; Guyer, R. B.; Brehm, J. H.; Barr, E. W.; Bollinger, J. M., Jr.; Krebs, C. *J. Am. Chem. Soc.* **2004**, *126*, 8108.
(11) Sinnecker, S.; Svensen, N.; Barr, E. W.; Ye, S.; Bollinger, J. M., Jr.; Neese, F.; Krebs, C. *J. Am. Chem. Soc.* **2007**, *129*, 6168.
(12) Hoffart, L. M.; Barr, E. W.; Guyer, R. B.; Bollinger, J. M., Jr.; Krebs, C. *Proc. Natl. Acad. Sci. U.S.A.* **2006**, *103*, 14738.
(13) Galonić, D. P.; Barr, E. W.; Walsh, C. T.; Bollinger, J. M., Jr.; Krebs, C. *Nat. Chem. Biol.* **2007**, *3*, 113.
(14) Galonić Fujimori, D.; Barr, E. W.; Matthews, M. L.; Koch, G. M.; Yonce, J. R.; Walsh, C. T.; Bollinger, J. M., Jr.; Krebs, C.; Riggs-Gelasco, P. J. *J. Am. Chem. Soc.* **2007**, *129*, 13408.
(15) Matthews, M. L.; Krest, C. M.; Barr, E. W.; Vaillancourt, F. H.; Walsh, C. T.; Green, M. T.; Krebs, C.; Bollinger, J. M., Jr. *Biochemistry* **2009**, *48*, 4331.
(16) Panay, A. J.; Lee, M.; Krebs, C.; Bollinger, J. M., Jr.; Fitzpatrick, P. F. *Biochemistry* **2011**, *50*, 1928.
(17) McDonald, A. R.; Que, L., Jr. *Coord. Chem. Rev.* **2013**, *257*, 414.
(18) Que, L., Jr. *Acc. Chem. Res.* **2007**, *40*, 493.
(19) Chiou, Y.-M.; Que, L., Jr. *J. Am. Chem. Soc.* **1995**, *117*, 3999.
(20) Ha, E. H.; Ho, R. Y. N.; Kisiel, J. F.; Valentine, J. S. *Inorg. Chem.* **1995**, *34*, 2265.
(21) Mehn, M. P.; Fujisawa, K.; Hegg, E. L.; Que, L., Jr. *J. Am. Chem. Soc.* **2003**, *125*, 7828.
(22) Mukherjee, A.; Cranswick, M. A.; Chakrabarti, M.; Paine, T. K.; Fujisawa, K.; Münck, E.; Que, L., Jr. *Inorg. Chem.* **2010**, *49*, 3618.
(23) Paine, T. K.; Zheng, H.; Que, L., Jr. *Inorg. Chem.* **2005**, *44*, 474.
(24) Das, O.; Chatterjee, S.; Paine, T. K. *J. Biol. Inorg. Chem.* **2013**, *18*, 401.
(25) Gibson, D. T.; Resnick, S. M.; Lee, K.; Brand, J. M.; Torok, D. S.; Wackett, L. P.; Schocken, M. J.; Haigler, B. E. *J. Bacteriol.* **1995**, *177*, 2615.

(26) Wolfe, M. D.; Parales, J. V.; Gibson, D. T.; Lipscomb, J. D. *J. Biol. Chem.* **2001**, *276*, 1945.
(27) Kauppi, B.; Lee, K.; Carredano, E.; Parales, R. E.; Gibson, D. T.; Eklund, H.; Ramaswamy, S. *Structure* **1998**, *6*, 571.
(28) Karlsson, A.; Parales, J. V.; Parales, R. E.; Gibson, D. T.; Eklund, H.; Ramaswamy, S. *Science* **2003**, *299*, 1039.
(29) Wolfe, M. D.; Lipscomb, J. D. *J. Biol. Chem.* **2003**, *278*, 829.
(30) Neibergall, M. B.; Stubna, A.; Mekmouche, Y.; Münck, E.; Lipscomb, J. D. *Biochemistry* **2007**, *46*, 8004.
(31) Tarasev, M.; Ballou, D. P. *Biochemistry* **2005**, *44*, 6197.
(32) Chen, K.; Costas, M.; Kim, J.; Tipton, A. K.; Que, L., Jr. *J. Am. Chem. Soc.* **2002**, *124*, 3026.
(33) Oldenburg, P. D.; Que, L., Jr. *Catal. Today* **2006**, *117*, 15.
(34) Oldenburg, P. D.; Feng, Y.; Pryjomska-Ray, I.; Ness, D.; Que, L., Jr. *J. Am. Chem. Soc.* **2010**, *132*, 17713.
(35) Costas, M.; Que, L., Jr. *Angew. Chem., Int. Ed.* **2002**, *41*, 2179.
(36) Suzuki, K.; Oldenburg, P. D.; Que, L., Jr. *Angew. Chem., Int. Ed.* **2008**, *47*, 1887.
(37) Bautz, J.; Comba, P.; de Laorden, C. L.; Menzel, M.; Rajaraman, G. *Angew. Chem., Int. Ed.* **2007**, *46*, 8067.
(38) Company, A.; Prat, I.; Frisch, J. R.; Mas-Ballesté, R.; Güell, M.; Juhász, G.; Ribas, X.; Münck, E.; Luis, J. M.; Que, L., Jr.; Costas, M. *Chem.—Eur. J.* **2011**, *17*, 1622.
(39) Bruijnincx, P. C. A.; Buurmans, I. L. C.; Gosiewska, S.; Moelands, M. A. H.; Lutz, M.; Spek, A. L.; van Koten, G.; Gebbink, R. J. M. K. *Chem.—Eur. J.* **2008**, *14*, 1228.
(40) Feng, Y.; Ke, C.-y.; Xue, G.; Que, L., Jr. *Chem. Commun.* **2009**, 50.
(41) Prat, I.; Mathieson, J. S.; Güell, M.; Ribas, X.; Luis, J. M.; Cronin, L.; Costas, M. *Nat. Chem.* **2011**, *3*, 788.
(42) Oloo, W. N.; Fielding, A. J.; Que, L., Jr. *J. Am. Chem. Soc.* **2013**, *135*, 6438.
(43) Kim, S. O.; Sastri, C. V.; Seo, M. S.; Kim, J.; Nam, W. *J. Am. Chem. Soc.* **2005**, *127*, 4178.
(44) Hong, S.; Lee, Y.-M.; Shin, W.; Fukuzumi, S.; Nam, W. *J. Am. Chem. Soc.* **2009**, *131*, 13910.
(45) Lee, Y.-M.; Hong, S.; Morimoto, Y.; Shin, W.; Fukuzumi, S.; Nam, W. *J. Am. Chem. Soc.* **2010**, *132*, 10668.
(46) Thibon, A.; England, J.; Martinho, M.; Young, V. G., Jr.; Frisch, J. R.; Guillot, R.; Girerd, J.-J.; Münck, E.; Que, L., Jr.; Banse, F. *Angew. Chem., Int. Ed.* **2008**, *47*, 7064.
(47) Li, F.; Van Heuvelen, K. M.; Meier, K. K.; Münck, E.; Que, L., Jr. *J. Am. Chem. Soc.* **2013**, *135*, 10198.
(48) Paria, S.; Que, L., Jr.; Paine, T. K. *Angew. Chem., Int. Ed.* **2011**, *50*, 11129.
(49) Polavarapu, P. L.; Fontana, L. P.; Smith, H. E. *J. Am. Chem . Soc.* **1986**, *108*, 94.
(50) *APEX 2*, version 2.1-0; Bruker AXS: Madison, WI, 2006.
(51) Sheldrick, G. M. *SHELXL-97, Program for crystal structure refinement*; University of Göttingen: Göttingen, Germany, 1997.
(52) Paria, S.; Halder, P.; Chakraborty, B.; Paine, T. K. *Indian J. Chem.* **2011**, *50A*, 420.
(53) Addison, A. W.; Rao, T. N.; Reedijk, J.; van Rijn, J.; Verschoor, G. C. *J. Chem. Soc., Dalton Trans.* **1984**, 1349.
(54) Paine, T. K.; Paria, S.; Que, L., Jr. *Chem. Commun.* **2010**, *46*, 1830.
(55) Mukherjee, A.; Martinho, M.; Bominaar, E. L.; Münck, E.; Que, L., Jr. *Angew. Chem., Int. Ed.* **2009**, *48*, 1780.
(56) Nam, W. *Acc. Chem. Res.* **2007**, *40*, 522.
(57) Lim, M. H.; Rohde, J.-U.; Stubna, A.; Bukowski, M. R.; Costas, M.; Ho, R. Y. N.; Münck, E.; Nam, W.; Que, L., Jr. *Proc. Natl. Acad. Sci. U.S.A.* **2003**, *100*, 3665.
(58) Kim, Y. M.; Cho, K.-B.; Cho, J.; Wang, B.; Li, C.; Shaik, S.; Nam, W. *J. Am. Chem. Soc.* **2013**, *135*, 8838.
(59) Smith, M. B.; March, J. *March's Advanced Organic Chemistry: Reactions, Mechanisms, and Structure*, 6th ed.; Wiley: New York, 2007; Vol. *11*.
(60) Fujita, M.; Costas, M.; Que, L., Jr. *J. Am. Chem. Soc.* **2003**, *125*, 9912.